Nano Energy 107 (2023) 108127

Contents lists available at ScienceDirect

Nano Energy

journal homepage: www.elsevier.com/locate/nanoen

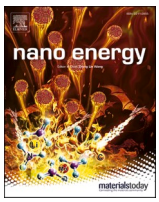

A stretchable, self-healing and semi-transparent nanogenerator for energy harvesting and sensing

Biswajoy Bagchi [a,b,1], Priyankan Datta [a,b,1], Carmen Salvadores Fernandez [a,b], Lulu Xu [a,b], Priya Gupta [a,b], Wei Huang [b], Anna L. David [a,c,d], Dimitrios Siassakos [a,c,d], Shervanthi Homer-Vanniasinkam [a], Manish K. Tiwari [a,b,*]

[a] Wellcome/EPSRC Centre for Interventional and Surgical Sciences, UCL, London W1W 7TS, UK
[b] Nanoengineered Systems Laboratory, UCL Mechanical Engineering, London WC1E 7JE, UK
[c] Elizabeth Garrett Anderson Institute for Women's Health, UCL, London WC1E 6AU, UK
[d] NIHR University College London Hospitals, BRC, 149 Tottenham Court Road, London W1T 7DN, UK

ARTICLE INFO

Keywords:
Hydrogel
Gold nanoparticles
Self-healing
Nanogenerator
Biocompatibility

ABSTRACT

Triboelectric nanogenerators (TENGs) with an ability to harvest mechanical energy from natural and human activities, have shown tremendous potential to realise self-powered electronic devices and sensors. However, in order for optimum utilization of biomechanical energy, TENGs need to have body or tissue mimicking properties without compromising performance. Herein, a new hydrogel based all-soft, self-healing and stretchable TENG is introduced which exhibits outstanding power generation capability surpassing existing competitors. This unique TENG is realized by using gold nanoparticles doped semi-transparent hydrogel as an electrode and Ecoflex as the triboelectric layer which integrates multifunctional properties including rapid self-healing in < 2 min, 900% stretchability, high conductivity, transparency and excellent biocompatibility with human dermal fibroblasts. The use of a gel electrode with both ionic and electronic conductivities underlines the importance of gold nanoparticles in enhancing the performance of soft TENGs. A 5 cm^2 device exhibits a prodigious power density of 1680 mWm^{-2} with an energy conversion efficiency of $\approx$ 26%, which is the highest achieved so far in contemporary hydrogel based TENGs. The moldable components allow easy fabrication of devices with tunable shapes and sizes that conforms to the human body and can power multiple electrical devices directly from body movements thus opening up possibilities for next generation self-powered wearable or implanted devices.

1. Introduction

Remarkable progress has been made in the development of wearable electronic gadgets, flexible sensor modules and health monitoring devices in recent times. Naturally, the search for alternative energy sources and new technologies to power these devices has increased concurrently with a conscious effort to transition toward self-powered devices [1–3]. Currently, wearable electronic devices rely heavily on conventional power sources like batteries which are rigid, non-renewable and often contain constituents that are hazardous for the environment. In this regard, an emerging technology based on electro-mechanical coupling is swiftly gaining prominence [3–6]. Since the advent of triboelectric nanogenerators (TENGs) in 2012, it has made a significant impact as a potential green device which can harvest electrical power from ubiquitous and wasted mechanical energy arising from natural phenomena (e.g., wind, waves), industrial processes (moving machine parts), transportation (moving vehicles) and daily human activities (running, exercising and body movements) [7–11]. Moreover, TENGs show a strong potential for developing self-powered sensor packages for monitoring diverse friction driven phenomena, and compared to the closely related piezoelectric nanogenerators (PENGs), exhibits several advantageous attributes such as low manufacturing cost and high power density [12–14]. Consequently, recent efforts are now directed to make TENGs even more suitable for practical applications by adding features such as stretchability, self-healing ability and transparency, which are especially important for implantable biomedical sensors, human-machine interfaces, robotics and energy harvesting devices [15–18]. However, it is extremely difficult to attain the

* Corresponding author at: Wellcome/EPSRC Centre for Interventional and Surgical Sciences, UCL, London W1W 7TS, UK.
E-mail address: m.tiwari@ucl.ac.uk (M.K. Tiwari).
[1] Denotes equal contribution.

https://doi.org/10.1016/j.nanoen.2022.108127
Received 30 September 2022; Received in revised form 4 December 2022; Accepted 19 December 2022
Available online 21 December 2022

above-mentioned features by using conventional electrodes such as copper/aluminium foils, sputtered coated gold, metallic nanowires, carbon nanotubes, graphene and indium tin oxide (ITO) due to the risk of degradation and delamination from the triboelectric layer over time [19]. Fabric and textile based TENGs with metal, carbon or conducting polymer electrodes offers good flexibility but suffer from mechanical robustness, limited stretchability, poor conductivity, high cost of production and are not self-healable or transparent [20]. Therefore, to address these issues, hydrogel-based electrodes have been introduced in TENGs which show remarkable stretchability, self-healing ability and transparency. Furthermore, hydrogels have shown additional benefits of being biocompatible and biodegradable [15,16,21–23]. For example, Li et al., synthesized a graphene oxide (GO) and laponite cross-linked conducting hydrogel electrode for TENG which is highly stretchable and self-healable with good power density under mechanical tapping (260 $mWcm^{-2}$) [24]. On a similar note, Luo et al., fabricated a MXene doped polyvinyl alcohol hydrogel based stretchable electrodes and reported a power density of 0.33 Wcm^{-2} [25]. Han et al., used gelatin cross-linked polyacrylic acid (PAA) to serve as a stretchable and self-healable electrode for single electrode TENG and showed a power density of 2.9 μWcm^{-2} [16] and Pu et al., prepared a PAAm-LiCl hydrogel as the electrification layer and electrode to fabricate a stretchable TENG, where a power density of 35 mWm^{-2} was achieved [26]. However, significant challenges with pure hydrogels are its low inherent ionic conductivity and dehydration, affecting the overall performance of TENGs [16,24,26]. Furthermore, synthesis of mechanically robust hydrogels especially which involves radical initiated crosslinking often requires multiple precursors (monomers, crosslinkers and photo-initiators) and high-power ultraviolet irradiation to promote crosslinking which increases cost and limit scalability [16,19,21,23,26,27]. Although organogels offers an attractive solution [28,29] in terms of dehydration resistance and biocompatibility, it would be interesting to investigate the effect of organic solvent – filler interaction on the gel properties.

In contrast, polyvinyl alcohol (PVA)-based hydrogels offer much simpler synthetic route, and they are ecofriendly, biocompatible and biodegradable [30,31]. Especially, borate crosslinked PVA hydrogels can be an ideal choice for a stretchable electrode for TENG due to their fast gelation, low cost, and potential self-healing properties [25,26]. However, as mentioned earlier, hydrogels have poor conductivity as it is dependent on the contribution from ions. For TENGs, the electrode should have reasonably high electrical conductivity to promote efficient charge collection. As electronic conductivity is much higher than ionic conduction, use of electrically conducting 'fillers' have been a successful strategy especially for hydrogel-based sensors which also enhances their physical attributes such as robustness, stretchability and self-healing [32]. Although a transparent TENG is difficult to achieve after doping with common conducting fillers such as graphene, carbon nanotubes and MXenes, a conducting 'filler' which does not drastically compromise the transparency is a potential solution.

Among conducting fillers, gold nanostructures with excellent electronic conductivity, optical properties and biocompatibility have been widely implemented in hydrogels but were mostly focused on biomedical applications such as scaffolds for tissue engineering, bioimaging, drug delivery, photothermal therapy, antigen detection, immunostaining and antimicrobial formulations [33,34]. Interestingly, little work has been done to make them applicable as stretchable electrodes for TENGs. For example, Lim et. al., used gold nanosheet impregnated polydimethylsiloxane (PDMS) as stretchable electrode for human motion detection [35]. and Park et. al., reported enhancement of TENG performance with electrodeposited gold nanoflower structures as electrodes; however, neither stretchability nor self-healing was investigated [36]. Thus, it is apparent that although conducting hydrogels have been researched extensively in developing stretchable electronics and sensors, their application as electrodes for TENGs and understanding their compatibility and interfacial interaction with different triboelectric surfaces is only recently gaining interest [17,19,37–42]. Specifically, metallic nanoparticle doped hydrogels present ample scope and potential, having both electronic and ionic contributions for developing next generation stretchable and self-healing TENGs with optimum mechanical properties and power density. This is a major opportunity which has not been exploited to date.

In the present work, we, for the *first time,* used gold nanoparticles (AuNp) embedded in PVA hydrogel to fabricate a fully soft, stretchable, self-healing and semi-transparent electrode for TENG. Addition of AuNps significantly enhances the charge collecting property of the hydrogel electrode by contributing towards electrical conductivity. Thus, we have successfully addressed a crucial problem i.e., low power output of hydrogel based TENGs by introducing synergistic contribution from both ionic (gel) and electronic (AuNps) parts in the electrode. This is made possible by the unique combination of two soft materials: Ecoflex (serving as the triboelectric layer) and a conducting hydrogel. Our TENG exhibits excellent output in terms of voltage, current and power density without compromising the properties of the hydrogel. Furthermore, the hydrogel electrode is sealed completely within the Ecoflex. This enables several benefits. First, the whole TENG surface is responsive under single electrode mode configuration, meaning it can respond to mechanical stimuli from both top and bottom surface of the device, which enhances the effective surface area and power density. Second, the device can withstand high mechanical force (45 N) from human finger/palm tapping and shows excellent stretchability (233%) over extended period of time. Third, the semi-transparent hydrogel electrode is able to fully self-heal rapidly giving stable performance and the compact sealing enables stable and close interfacial contact between soft Ecoflex and hydrogel, enabling optimum charge collection during energy harvesting. Fourth, being encapsulated by the elastomer, dehydration of the hydrogel is prevented thereby enhancing the lifetime of the device. Lastly, incorporating gold nanoparticles enhances the conductivity of the hydrogel electrode without substantially affecting stretch, self-healing ability and transparency. The soft and pliable nature of the hydrogel electrode can be exploited to design TENGs of any desired shape. For example, we have fabricated TENGs in the shape of a sphere and a narrow flexible rod by encapsulating the hydrogel inside Ecoflex, which allows multidirectional contact-separation and potentially opening-up more practical ways of sensing and energy harvesting capabilities from the device.

We demonstrate multiple potential applications and capabilities of our device based on different shape and form, specifically, harvesting energy from human body movements like finger tapping, arm bending and foot tapping which were used to self-power electrical devices like LEDs, capacitors, digital calculator and a thermometer without using any batteries or external power. Interestingly, using the spherical TENG, we were able to harvest energy directly from the palm of the hand by using it as an 'anti-stress' ball exercise which can instantaneously power up 60 LEDs and charge capacitors just by softly pressing the ball. The gel is non-cytotoxic to human fibroblast cells as demonstrated by the Live/Dead test which again highlights the potential broad spectrum capability of the device in biomechanical energy harvesting either in *ex vivo* or *in vivo* conditions.

2. Experimental section

2.1. Synthesis of gold nanoparticle doped PVA hydrogel

Gold nanoparticles (AuNp) were initially synthesized by in situ reduction with tannic acid in the PVA matrix followed by crosslinking with borate to form the doped hydrogels. Briefly, 8 wt% PVA (3 mL) (Sigma Aldrich) solution was stirred at 1000 rpm at 95 °C for 5 mins. Next, measured volume (0.08–2 mL) of 10 mM gold(III) chloride trihydrate ($HAuCl_4 0.3\ H_2O$) (Sigma Aldrich) solution was added dropwise while stirring. After brief mixing, 50–100 μL of 6 (mM) tannic acid (Thermofisher Scientific) was added. The colour of the solution rapidly

turned wine red indicating formation of AuNp [43]. The hydrogel was formed by thoroughly mixing 4 wt% sodium borate ($Na_2B_4O_7$) (3 mL) (Sigma Aldrich) with the above solution at room temperature. The hydrogel was then stored for 1 h to complete reaction and then soaked in distilled to wash away excess reactants [44,45]. Finally, the gel was purged with N_2 gas to remove water from the surface. Based on the concentration of gold salt used, the PVA-borate hydrogels have been designated as G0 (without gold), G1 (0.1 mM), G2 (0.5 mM), G3 (1.5 mM), G4 (2 mM) and G5 (2.5 mM).

2.2. Fabrication of TENG

To fabricate the TENG, a certain volume of Ecoflex-0050 silicone rubber (part A and part B) was thoroughly mixed, degassed and then poured into a teflon mould. Next, the Ecoflex was partially cured at 100 °C for 5 mins. A conducting silver thread was then attached on top of Ecoflex and thereafter the previously made hydrogel was cut into a rectangular slab of 2.5 cm × 2 cm and placed on the Ecoflex layer. Next, another layer of Ecoflex was poured on top of the hydrogel and left to cure at room temperature for 24 h to form the TENG. Finally, the TENG was peeled off from the mould as a flexible film of thickness 1.5 mm and effective area of ≈ 5 cm^2. Flexible TENGs of different shapes (wrist band and anti-stress ball) were fabricated using pre-made moulds as shown in figure S1 (ESI†). Degassed Ecoflex was poured in part I of the mould followed partial curing and addition of hydrogel embedded with silver thread. Next part II of the mould was put on tightly and Ecoflex is again added through the opening on top to fill the mould. The mould is left to cure at room temperature after which it is dismantled to get the TENG.

2.3. Material characterization and electrical measurements

The AuNp doped PVA hydrogels were characterized using UV–visible spectroscopy (Orion AquaMate 8100), transmission electron microscopy (TEM, Jeol 2100), scanning electron microscopy (SEM EVO 10), Instron tensile strength tester (Instron 5969) and fourier transform infrared spectroscopy (FTIR, Nicolet iS50). For TEM, gel samples were first ultrasonicated before mounting on copper grid. For SEM, the gels were freeze-dried before observing under microscope. In case of FTIR, the gels were first dried, and a small portion was used with attenuated total reflectance (ATR) attachment. The electrical resistance of the hydrogels (cut into a dimension 1 cm × 1 cm × 0.5 cm) was measured by a digital multimeter (RSDM 3055) by attaching two aluminium foils as electrodes on opposite side of the hydrogels. Output voltage was measured using a digital oscilloscope (MDO3024, Tektronix). The current and charge were measured using an electrometer (6517B Keithley). The force applied during tapping was calibrated using a force plate (FP3, Biometrics Ltd). The device was directly placed on the force plate and the tapping force was increased (up to 80 N) gradually while recording the voltage and current output. For the stability assessment, the TENG was impacted with 45 N force at 1 Hz frequency using a pneumatic linear actuator fitted with polyethylene sulphone (PES) membrane (as the counter triboelectric surface) and controlled by Arduino. For the above measurements, a rectangular (dimension- 2.5 cm × 2 cm) TENG was used. The resistance of the gel was measured after specific intervals by cutting it out of the Ecoflex layer. For tensile strength measurement, G3 TENG of length 5 cm and cross-sectional area 0.5 cm^2 (made using the mould described before) was mounted between two clamps and stretched at a rate of 20 mm per minute. Young's modulus was then calculated from the stress vs strain curve. For performance analysis under self-healing cycles, the hydrogel inside the Ecoflex was separated into two halves (by pressing and pulling the hydrogel apart) and then voltage and current were measured under load resistance of 10^8 Ω before and after each self-heal cycle. For temperature dependent performance analysis, the TENG was incubated on a hot plate at various temperatures (25–100 °C) for 15 min and then voltage and current were measured under 10^8 Ω. To determine effect of stretchability on TENG performance, the TENG (in size: 6 cm × 1 cm) was stretched (0–200%) by fixing clamps on two ends and then tapped with a force of 45 N. Voltage and current were measured as above. Finally, power density was calculated and compared (with respect to normal condition) to determine TENG performance (%).

All the participants have given written consent for their involvement during energy harvesting and sensing demonstrations using the device. To demonstrate detection of body movement, a rectangular TENG strip (size: 6 cm × 1 cm) was attached (via adhesive tape) directly at various locations (finger joint, wrist, elbow, neck and knee-cap) on body of healthy volunteers. The voltage was then measured in response to the specific movements by digital oscilloscope.

2.4. Biocompatibility assessment

Cytotoxicity study was performed on human dermal fibroblast (HDF) cell lines, where the cells are cultured in DMEM media supplemented with FBS (10%) and antibiotic (PSN) (1%) at 37 °C in a humidified atmosphere with 5% CO_2. After 75–80% confluency, cells were harvested with trypsin (0.025% v/v) and EDTA (0.52 mM in PBS) and were seeded at desired density to allow them to re-equilibrate for a day before the start of experimentation.

Approximately 0.2 g of G3 hydrogel was weighed and sterilised beforehand by washing with absolute ethanol and later UV exposure for 20 min. Next, cells were seeded at concentration of 10^5 cells/mL in a 6 well plate and were then incubated with the hydrogel for 72 h. After incubation, the hydrogel piece was taken out and the cells were washed with PBS twice and 50 μL from the LIVE/DEAD (L3224, Thermofisher Scientific) assay stock solution (Calcein AM (2 μM) and Ethidium homodimer (4 μM)) was added to the petridish. After 5 min, the cells were again washed with PBS to get rid of the excess dye and thereafter fluorescence images were taken using a fluorescence microscope (EVOS M5000) to evaluate the viability of the cells.

3. Result and discussion

The hydrogels were synthesized by a simple one-pot technique by first forming gold nanoparticles in the PVA solution followed by crosslinking with borate ions as represented in Fig. 1a. In the first step, the gold nanoparticles were formed by in situ reduction of gold salt by tannic acid, a well-known eco-friendly antioxidant. The polyphenolic functional groups in tannic acid serves as an efficient reducing and stabilising agent which in the present case helps in uniform dispersion of the nanoparticles in PVA [43]. This 'green' synthetic approach, thus, avoids environmentally toxic reducing agents such as hydrazine or sodium borohydride [46]. Moreover, the reduction is very fast and typically takes less than 2 mins to completion. In the second step, borate was mixed at room temperature to promote crosslinking and hydrogel formation [47].

The formation of the gold nanoparticles is confirmed from the UV–visible spectra of PVA suspensions (Fig. 2a). As can be observed from Fig. 2a, the intensity of the surface plasmon resonance (SPR) peak (for gold nanoparticles) at 530 nm increases from G1 to G3, indicating formation of progressively higher concentration of nanoparticles. However, a shift in the peak towards longer wavelength is observed for G4 and G5 which appears at 540 nm. This is because of possible formation of nanoparticle agglomerates due to high concentrations. An approximate particle size was determined from the position of the SPR peak. Here, peak at 525 nm indicates nanoparticle size of around 15 nm for G1-G3 and much larger size (40 nm) for G4 and G5 [48]. It is to be noted that for G4 and G5, a higher baseline absorbance is observed around 800 nm- this is probably due to scattering from agglomerated PVA gel particles in these samples during measurement. This is also evident from the colour of the respective PVA-nanoparticle suspensions (Fig. 2b), where G1-G3 have wine red coloration while it shifted to violet-blue region of the visible spectrum for G4 and G5 [49]. The

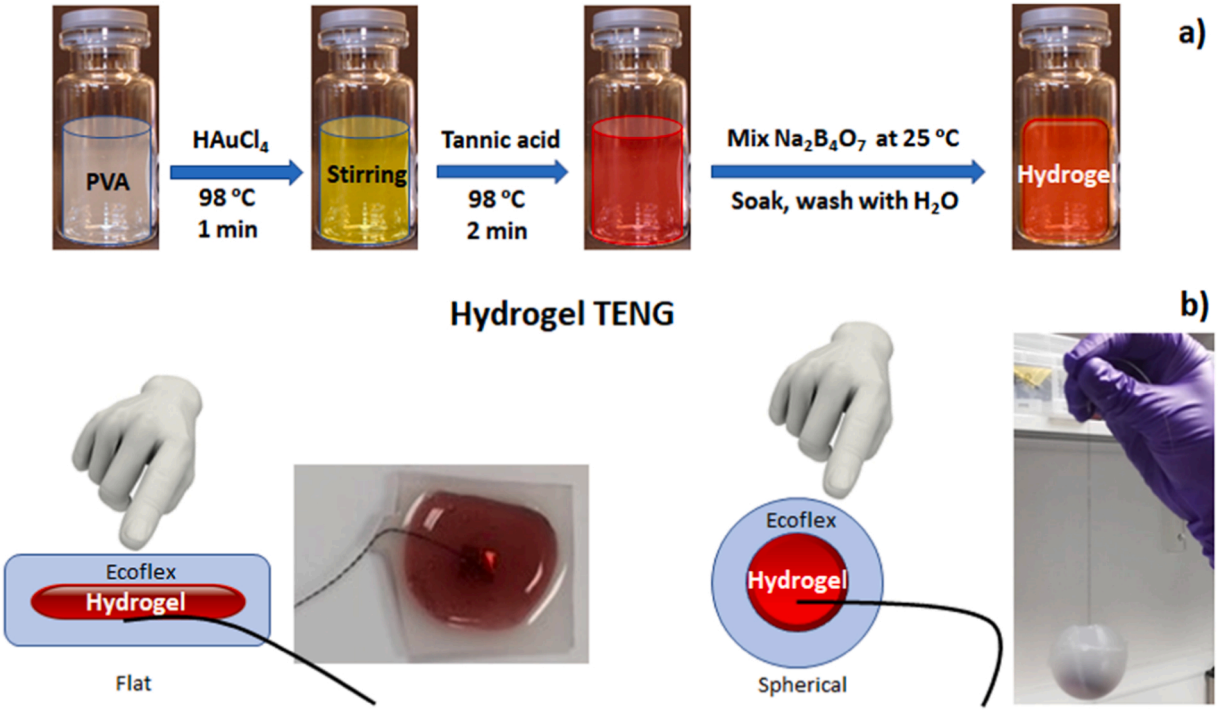

Fig. 1. Schematic showing a) synthesis of AuNp doped hydrogel, b) Design of TENGs of different shapes.

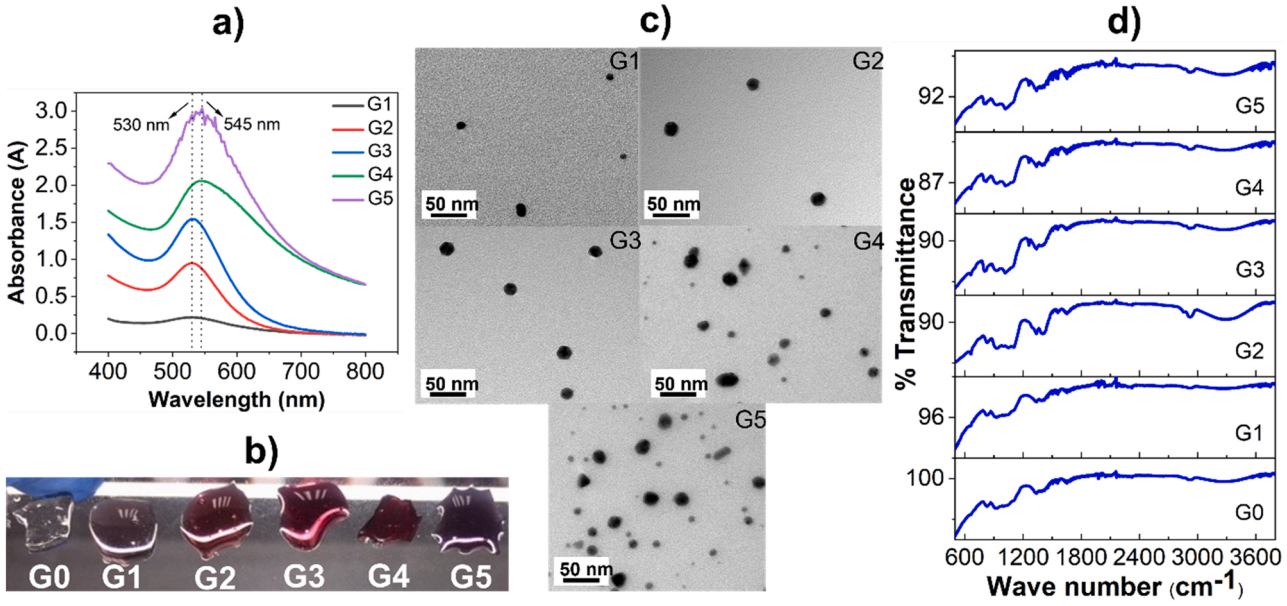

Fig. 2. a) UV–visible spectra of the Au-Np-PVA precursor solution (G1-G5), b) photographic images of the gels (G0-G5), c) Transmission electron microscopy (TEM) images of the gels (G1-G5) and Fourier transform infrared spectra of the dried gels (G0-G5).

particle size was further confirmed through transmission electron microscopy (TEM) which shows uniform distribution of spherical gold nanoparticles in PVA with sizes range of 10–15 nm for G1-G3. However, as expected, G4 and G5 shows higher particle number density particle due to increased concentration. Both smaller (5 nm) and larger (20–25 nm) sized particles can be observed. The larger sized particles are formed due to agglomeration, which is reflected in the shift of their SPR peak (Fig. 2a).

The interaction between different functional groups, which contributes toward crosslinked hydrogel was investigated by Fourier transform infrared spectroscopy (FTIR). Fig. 2d shows the FTIR spectra of the synthesized hydrogels. PVA gives peak around 840 cm^{-1} due to the out-of-plane vibration of C-C groups and broad peak at 1000–1150 cm^{-1} is attributed to the stretching vibrations of C–O and C–O–C groups. PVA-borate crosslinking is indicated by the appearance of peaks around 1336 cm^{-1}, 1460 cm^{-1} (asymmetric stretching relaxation of B-O-C) and 640 cm^{-1} (B-O-B linkage) in all the hydrogels. Presence of hydroxyl groups are detected by the broad peak around 3200–3600 cm^{-1} [44,45]. However, in case of doped hydrogels, peak around 1250 cm^{-1} and 1640 cm^{-1} indicates the ester moiety and the C═C stretching vibrations in the tannic acid structure. More importantly, in contrast to G0, an increase in the intensity of the broad peak

around 3200–3600 cm^{-1} indicates strong hydrogen bonding interaction between tannic acid and PVA through multiple hydroxyl groups [50–52]. Thus, the doped PVA hydrogels are dual crosslinked with borate and tannic acid molecules. No additional peaks were observed due to AuNps as they are coated with tannic acid. Fig. 3a-c, shows the scanning electron microscopy images of G1, G3 and G5 which reveals a porous microstructure characteristic of freeze-dried gels. Elemental mapping (Fig. 3d-f) of the same samples shows the distribution of AuNps (green spots in the image) in the gel matrix. To minimize the interference of other elements we only traced the distribution of carbon and gold in the hydrogel. As expected, the concentration of AuNp progressively increases from G1 (Fig. 3d) to G5 (Fig. 3f). Based on above, Fig. 3g shows the proposed intermolecular interactions between the components that lead to the formation of the crosslinked hydrogel. Specifically, dynamic intra and intermolecular chemical crosslinks occurs between PVA chains, diol moieties and borate ions while tannic acid is primarily involved in non-covalent interactions through multiple hydrogen bonding with PVA [44,50–52]. All these interactions resulted in a crosslinked gel with self-healing and stretchable properties.

For the hydrogel to serve as an efficient electrode for TENG, it needs to have high electrical conductivity. While pure PVA-borate hydrogel is conducting due to presence of sodium and borate ions, it is still much less than typical electronic conductors [53]. Therefore, we hypothesised that addition of metallic nanoparticles might substantially enhance it due to the formation of conducting pathways and the hydrogel will benefit from both ionic and electronic contributions. AuNps was selected based on its easy synthesis, resistance to oxidation, optical properties, nontoxic nature and high electrical conductivity [33,34]. The resistances of individual hydrogels (G0-G5) were measured and as can be seen from Fig. 4a, compared to G0 (130 $k\Omega cm^{-1}$), the resistance significantly decreased with increased concentration of AuNps with the lowest resistance observed for G3 (10 $k\Omega cm^{-1}$). Interestingly, G4 and G5 exhibit higher electrical resistances (45 $k\Omega cm^{-1}$ and 70 $k\Omega cm^{-1}$ respectively) despite containing high density of AuNps. As reported by Chan et. al. [54], this is probably because high concentration of AuNps causes local agglomerates (as evident from TEM image in Fig. 2c and elemental mapping in Fig. 3f) which leads to the formation of large tunnelling gaps between individual nanoparticles and reduces the number of effective conducting pathways for AuNps inside the hydrogel. This is schematically explained in figure S2 (ESI†), where, as we proceed from low to high concentration of nanoparticles, the tunnelling gap increases due to cluster formation which restricts formation of conductive

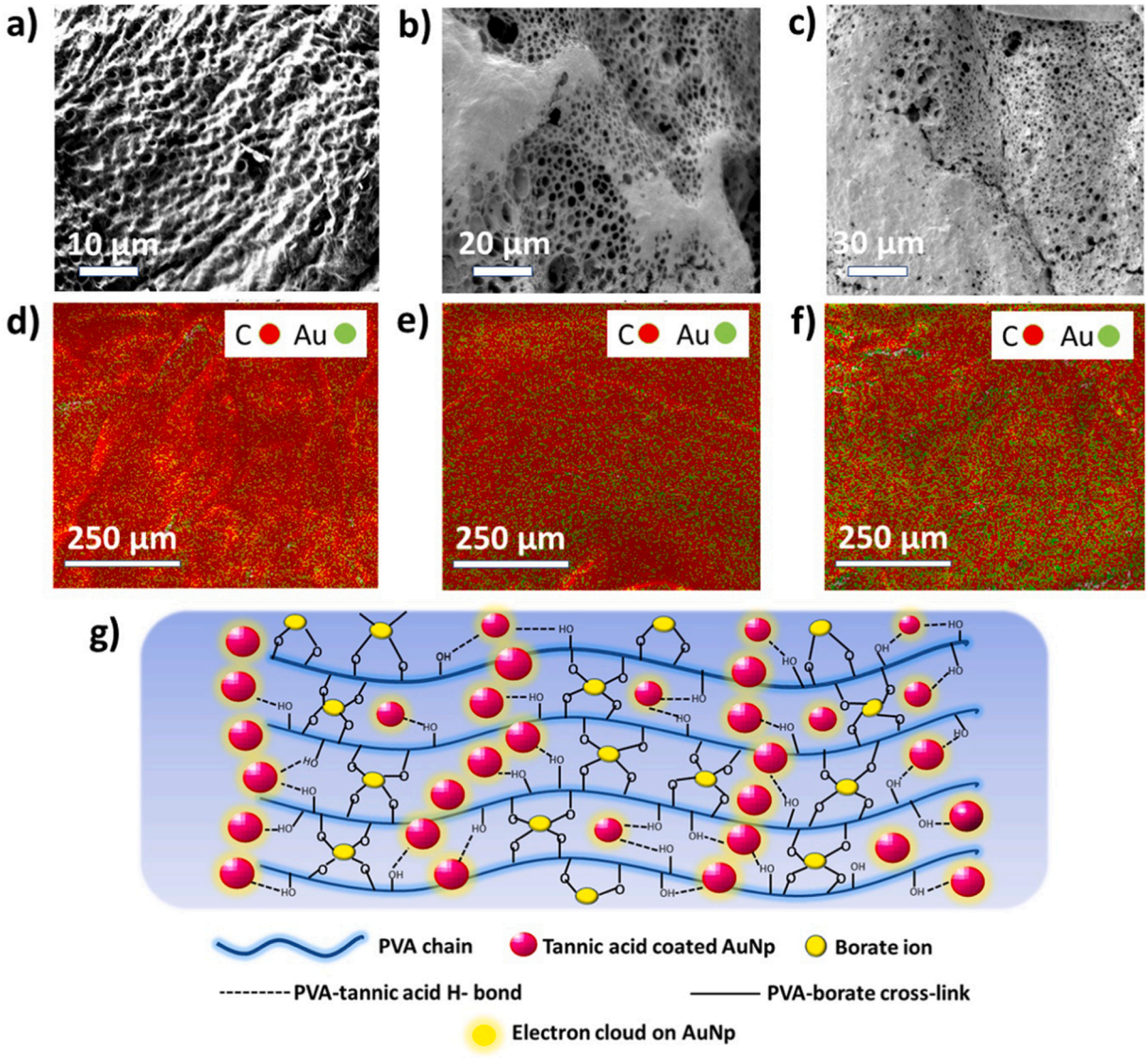

Fig. 3. SEM image of doped hydrogels showing microstructure of a) G1, b) G3 and C) G5. Corresponding elemental mapping of the samples showing distribution of AuNp (in green) in d) G1, e) G3 and f) G5 and g) schematic representation of the intermolecular crosslinking in the AuNp doped hydrogel.

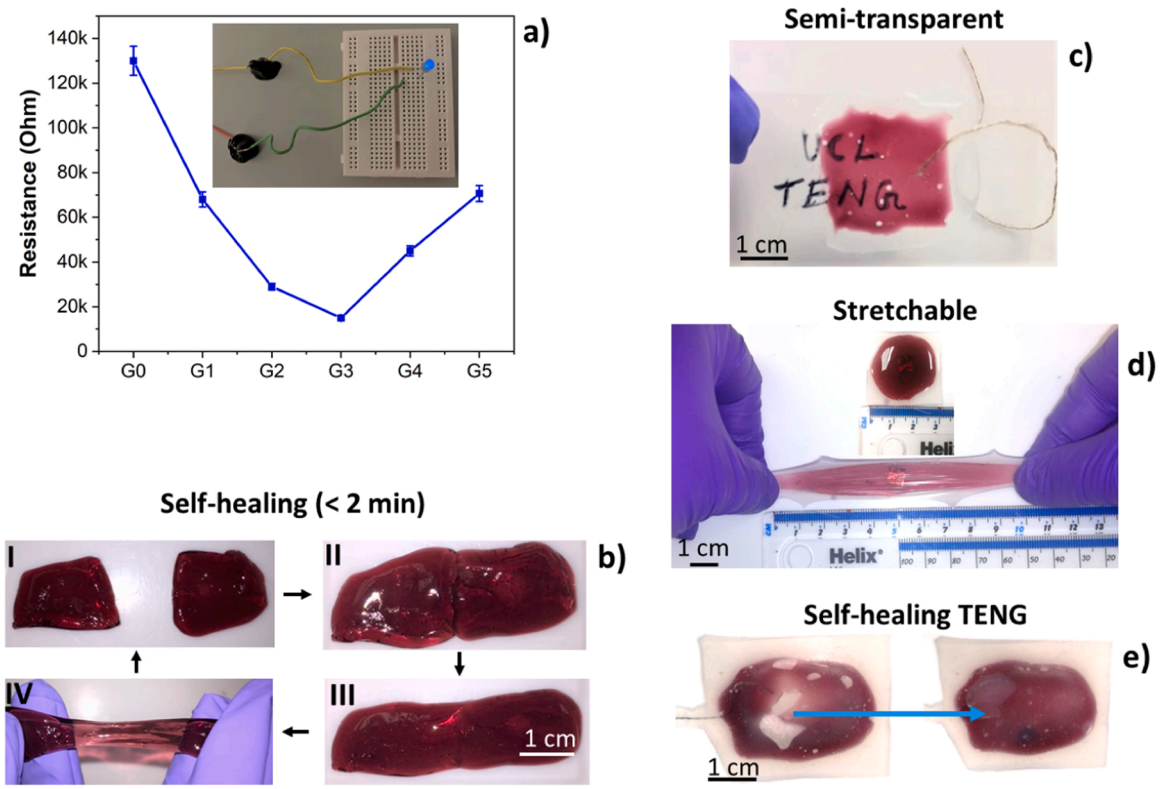

Fig. 4. a) Electrical resistance variation in the hydrogels (G0-G5), b) self-healing capability of the G3 hydrogel, c) semi-transparent nature of the G3 hydrogel, d) stretchability (233%) of G3 TENG and e) self-healing of G3 inside the TENG after repeated tapping with a force of 45 N.

pathways. Thus, G3 hydrogel with optimum distribution of AuNPs significantly improves the electrical conductivity as compared to pure PVA-borate hydrogel. This conducting nature is shown by using G3 as a conducting interconnect which then lights up a LED (inset Fig. 4a and video S1, ESI†).

Supplementary material related to this article can be found online at doi:10.1016/j.nanoen.2022.108127.

Dynamic intermolecular crosslinking and hydrogen bonding interactions between PVA, borate ions and tannic acid endows the hydrogel with excellent self-healing properties [31,53,55]. To demonstrate, we cut G3 hydrogel (length 4 cm and thickness 1.5 cm) in half and the two parts of the gel were joined together at room temperature within a very short span of time (< 2 mins) which can be stretched without breakage (Fig. 4b and video S2, ESI†). The process was repeated 50 times and 100% self -healing was achieved after every cycle. Additionally, G3 TENG is semi-transparent, where the words 'UCL TENG' written on a clean polyethylene terephthalate (PET) sheet is clearly visible when placed under the hydrogel TENG (thickness of the gel is 0.1 cm) and this may be suitable for applications such as an energy harvesting layer on glass windows, doors, roofs etc. (Fig. 4c). It is however to be noted that the transmittance value when measured by UV–visible spectroscopy shows a broad range of 60–80% (figure S3, ESI†). The lower transmittance at 530 nm is attributed to the SPR absorption peak of AuNps and not due to opacity [47]. G3 also exhibit high stretchability of ≈ 900% as shown in the video S3 (ESI†) which in turn makes the TENG based on it, stretchable up to ≈ 233% (Fig. 4d, inset showing original length of the TENG). This is made possible by seamless and efficient packaging of two soft and stretchable materials, i.e., Ecoflex and the hydrogel where the Ecoflex fully encapsulates the hydrogel thereby adding robustness to the device. An interesting feature of the TENG is that sometimes after prolonged tapping (after 8,000 cycles) with a force of 45 N, the hydrogel electrode (shown for G3) shows breakage and this is possibly due to the high imparting force applied, however, the gel is able to fully self-heal inside the Ecoflex packaging (Fig. 4e) after 10 mins and recovers its functional/stable operation. This is represented in figure S4 (ESI†) where the TENG performance is regained close to 100% after 20 'cut and self-healing' cycles. It is to be noted that when the gel is separated (cut) inside the Ecoflex, it can still behave as an electrode as the silver cable is attached to the other half of the gel; however, the effective electrode area is now reduced (almost halved) resulting in lower performance (around 65%). As demonstrated by Luo et. al. [25], sealing with Ecoflex effectively prevents loss of water from the hydrogel preserving the self-healing nature and performance of the TENG. Thus, all the desired mechanical and electrical properties of a practical TENG are met when G3 is used as the stretchable electrode.

Supplementary material related to this article can be found online at doi:10.1016/j.nanoen.2022.108127.

Output performance of the TENG was investigated in detail with respect to human finger touch and body movements. The TENGs were repeatedly tapped with finger while connected to different load resistances (R_L) (10^3-10^9 Ω). Fig. 5a, shows the effective maximum power density obtained (power density = $(I_L \times V_L)/A$, where, I_L is the current, V_L is the voltage drop under load 10^8 Ω and A is the area) for each hydrogel TENG, with a tapping force of 45 N and frequency of 1 Hz. It is interesting to note that with increase in gold nanoparticle concentration (from G1 to G5), the effective power density gradually increases and reaches a maximum for G3 and then decreases. This is possibly because G3 has the least electrical resistance which serves as an optimum current collector as also evident from the voltage and current generated for each gel composition where G3 with the lowest resistance produces the highest output (figure S5, ESI†). While for G5 and G6, less conductive pathways (formed due to particle agglomeration) leads to poor performance. However, compared to G0 (0.6 Wm^{-2}), all the TENGs show higher power density at 10^8 Ω (see Fig. 5a). G3 TENG, with a power density of 1.68 Wm^{-2} significantly outperforms previously reported hydrogel based TENGs, with or without different fillers (see Table S1, ESI†). Fig. 5b shows the variation of current (I_L), voltage (V_L) and effective power density for G3 across different load resistances. As

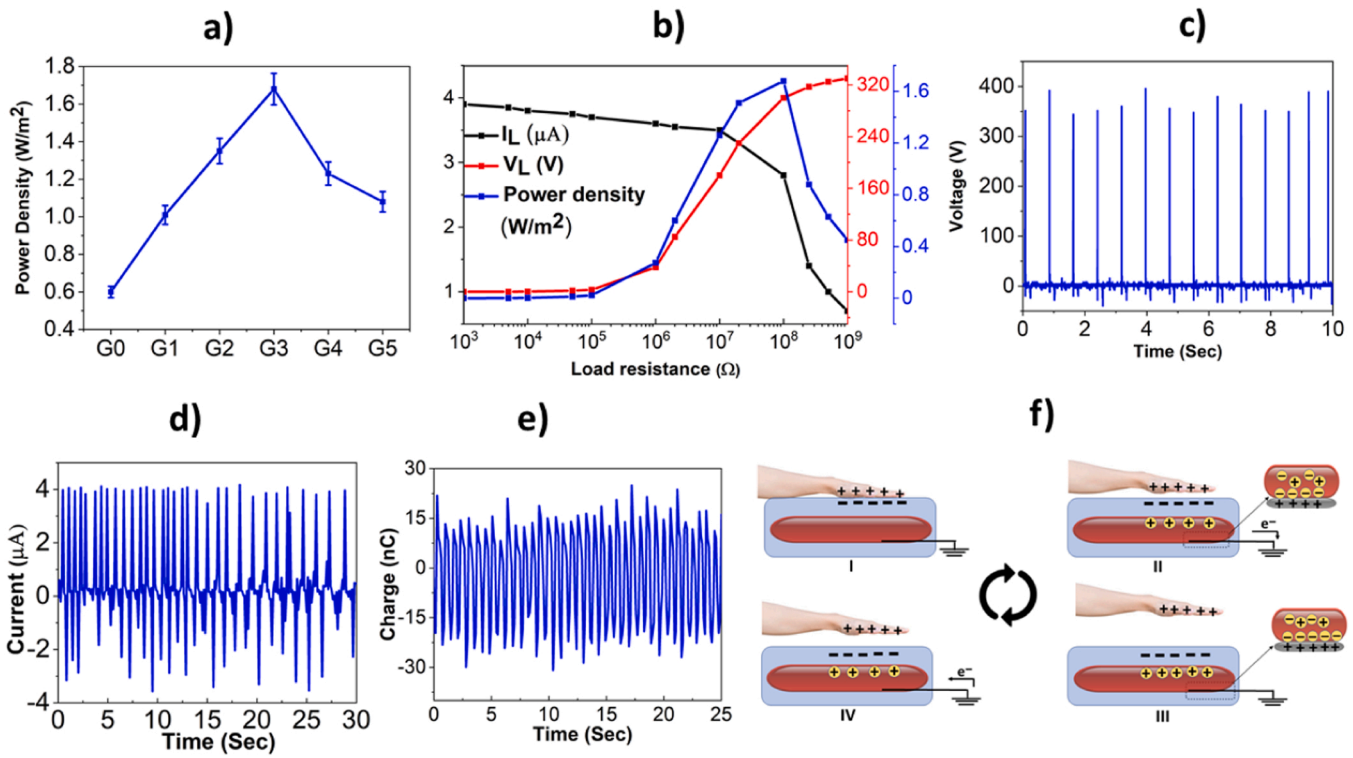

Fig. 5. a) Variation of power density in the hydrogel TENGs, b) variation of output voltage, current and power density with load resistances for G3 TENG, c) V_{oc}, d) I_{sc}, and e) Q_{sc} for G3 TENG and f) working mechanism of the TENG under singe electrode mode configuration. The tapping was done with a force of 45 N at a frequency of 1 Hz.

expected, instantaneous voltage increased and gradually reached a peak, while the corresponding current measured across load decreased. Fig. 5c, d and e, shows the corresponding open circuit voltage (V_{oc}), short circuit current (I_{sc}) and the amount of charge transferred under short circuit condition (Q_{sc}) from G3 under similar tapping condition. The TENG performance (V_{oc} of 384 V, I_{sc} of 4 μA, Q_{sc} of 45 nC (charge density of 90 μCm^{-2}) and a peak power density of 1.68 Wm^{-2}) clearly demonstrates the superior capability compared to G0 (V_{oc} of 180 V, I_{sc} of 2.5 μA, Q_{sc} of 25 nC and power density of 0.6 Wm^{-2}). Furthermore, comprehensive literature survey shows that the performance of G3 is the best in class compared to previous hydrogel based stretchable electrodes (see Table S1, ESI†). The stability of the TENG is also demonstrated for 10,000 cycles, where a stable V_{oc} of 80 V is obtained under a tapping force of 45 N and frequency of 1 Hz (figure S6 and video S4, ESI†). The voltage obtained in cyclic tests is lower because the polyethylene sulphone (PES) membrane used as the counter surface is triboelectrically less positive than human skin [7–9]. The resistance of G3 (measured after definite intervals) shows negligible variation even after prolonged operation indicating stability of the gel electrode (figure S7a, ESI†). Furthermore, the resistance remained stable even after 20 'cut and self-healing' cycles indicating stability of the gel structure (figure S7b, ESI†). As for the mechanical properties, the stretchable TENG exhibits a Young's modulus of 0.246 MPa after 10,000 cycles calculated from the slope of the stress vs strain curve (Figure S8a and b, ESI†) which highlights the robustness of the device obtained through effective sealing of the hydrogel inside the Ecoflex. Cyclic tensile test was also done to evaluate the effectiveness of self-healing hydrogel inside Ecoflex. Figure S8c (ESI†) shows the force vs displacement (100% strain) curve for G3 TENG. As evident, the device regains mechanical properties quite efficiently after 10 self-healing cycles. To further evaluate the stability of the hydrogel TENG, performance analysis was carried out by varying temperature and stretching state of the device. As evident from figure S9 (ESI†), the output efficiency of the TENG gradually decreases to 70% when the temperature was varied from 25 °C to 100 °C. This is because with increase in temperature the resistance of the electrode increases due to increased collision between electrons and ions in the hydrogel resulting in poor charge collection and performance. However, for most bio-mechanical energy harvesting (especially with implanted devices) applications, the temperature will not exceed 45 °C and hence it is expected that the device should be stable in the 25–45 °C range. When the device was stretched at various lengths (0–200%), the output performance initially drops and then seems to stabilise at 80% for 200% stretch condition (figure S10, ESI†). This might be due to the interplay between two opposing factors: at stretched condition, increased separation between AuNps in the hydrogel leads to lower conductivity of the electrode layer and this results in decrease in TENG performance. However, as stretching continues, the area of contact between skin and Ecoflex layer also increases generating higher triboelectric charges at the interface. Hence the observed stabilisation effect is a reflection of simultaneous opposing change in resistance and contact charge generation in the stretched device. The working mechanism of the TENG (using G3 as the electrode) under human hand tapping is schematically represented in Fig. 5f. In single electrode mode, initiated by the physical contact of the skin during tapping on Ecoflex surface, opposite charges are generated on the Ecoflex layer and human skin due to triboelectrification. The Ecoflex surface is negatively charged, meanwhile the skin acquires positive charge (I). At this stage there is no electrical potential difference as the charges are balanced. Once the skin starts to separate from the Ecoflex layer, unscreened negative charge on the Ecoflex induces positive ions (H^+ and Na^+) in the hydrogel layer to move at the Ecoflex-hydrogel interface. Simultaneously, an electrical double layer is formed at the hydrogel-silver wire interface with the same amount of negative ions (mainly Cl^- from the gold salt ($HAuCl_4 0.3\ H_2O$) in the hydrogel and positive charges on the metallic wire. As a result, electrons would flow from the electrode to the ground through an external circuit, producing an electrical signal (II). When the skin is separated further from the Ecoflex layer, the induced positive charges in the gel would fully neutralize the negative charges on Ecoflex layer and

no signal is generated (III). Finally, when the skin approaches the Ecoflex layer again, the process is reversed i.e., electrons now start flowing from the ground to the electrode forming an opposite electrical signal (IV). This process gets repeated generating an alternating current or voltage signal [26]. Presence of metallic gold nanoparticles is implicated to play two important roles, first it serves as a source of free electrons in the gel and second it provides conducting pathways. These two factors significantly enhance (≈ 180%) the power density of G3 TENG compared to pure PVA gel based TENG which rely only on ionic conduction.

Supplementary material related to this article can be found online at doi:10.1016/j.nanoen.2022.108127.

Since G3 hydrogel TENG exhibit highest power density, we used them to demonstrate several aspects of energy harvesting from human body movements accentuating the versatility of the soft and flexible device (Fig. 6). For instance, when the TENG is applied on the arm, the bending motion can directly power up 15 LEDs instantly (Fig. 6a and video S5, ESI†), while gentle finger tapping on the TENG generates enough power to light up 120 LEDs (Fig. 6b and video S6, ESI†). Similarly, the TENG is robust enough to withstand the pressure from a foot i.e., when placed on the heel of a flip-flop, it powers up 65 LEDs upon repeated tapping with the heel of the foot (Fig. 6c and video S7, ESI†). Furthermore, to make it easier to harness mechanical motion from human activities, two unique designs namely, a spherical shaped soft 'anti-stress' ball and a rod-like TENG (which can be used as a wristband) is fabricated, both of which can light up to 60 LEDs directly upon gentle repeated touch (Fig. 6d and e) and (video S8 and S9, ESI†). Figure S11 (ESI†) summarizes the V_{oc} and I_{sc} obtained during arm bending (figure S11a and d), foot tapping (figure S11b and e) and pressing of 'anti-stress' ball (figure S11c and f). In order to power electronic devices with the TENG, a rectifier circuit used so that the alternating current could be converted to direct current through (figure S12, ESI†). Using this circuit, the TENG could charge different capacitors (1 μF, 4.7 μF and 10 μF) within 120 s when tapped with a frequency of 2 Hz (Fig. 6f). As a practical application, when a 10 μF capacitor is charged to 5.3 V by the TENG (size: 5 cm × 4 cm) upon continuous tapping for 170 s (figure S13, ESI†), the harvested energy could power the LCD screen of a digital calculator (Fig. 6g and video S10, ESI†) and thermometer (Fig. 6h and video S11, ESI†) for few seconds. Obviously, the energy generation rate was not fast enough to compensate for the energy consumption by the electronic devices. However, larger device designs should make that possible.

Supplementary material related to this article can be found online at doi:10.1016/j.nanoen.2022.108127.

Taking advantage of the soft and stretchable nature of the TENG, we are able to detect movement of joints in human body. The friction between the skin and the TENG patch generates reproducible voltage signal patterns during specific body movements (Fig. 7 and video S12, ESI†). Processing such patterns can be useful to monitor and diagnose diseases associated with musculoskeletal system. Considering the biomechanical sensing and energy harvesting applications from human body it is also important to assess the working range of the device under different applied forces. Figure S14a (ESI†) shows the variation of output voltage with applied pressure on the sensor. The applied pressures were varied in kilo pascal range in order to assess sensitivity under gentle joint movements. As evident from the slope of the graph (figure S14a, ESI†), G1 has a sensitivity of 0.36 V/kPa while G3 and G5 have higher sensitivities (0.53 and 0.56 V/kPa respectively), and this is again probably due to the presence of increased gold nanoparticles in G3 and G5. We measured sensitivities only for G1, G3 and G5 as they have the highest disparity in AuNp concentrations following on from elemental mapping images (see Fig. 3d-f). Figure S14b (ESI†) shows the variation of power density with tapping force in the range of 5–80 N for G3 TENG (G3 was selected as it showed highest performance (see Fig. 5a). The power density initially increases with applied force and then stabilises around 80 N, which indicates the electrical output limit of the device.

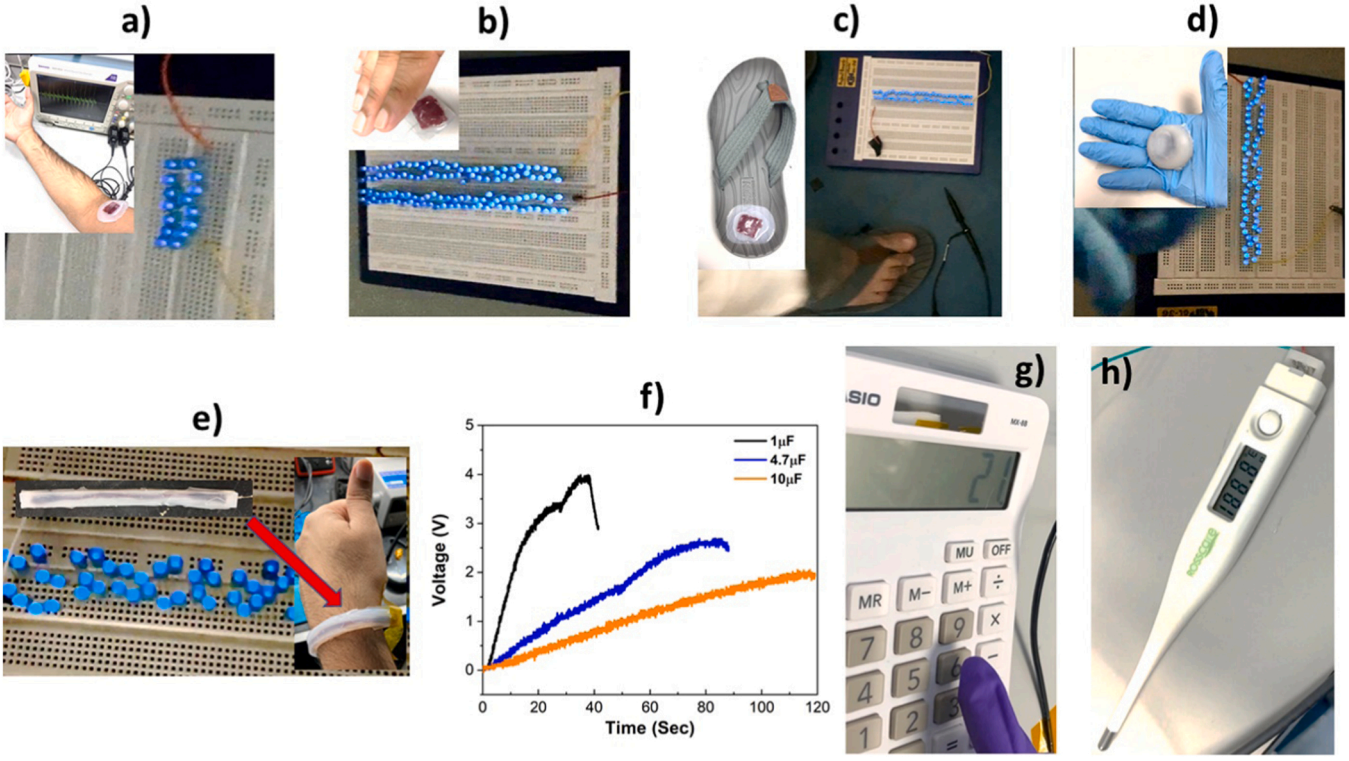

Fig. 6. Demonstrations of the energy harvesting capability using G3 TENG- powering blue LEDs from a) arm bending (inset showing TENG attached to the bicep), b) finger tapping (inset showing tapping), c) foot tapping (inset showing TENG attached on the heel segment of the flip-flop, d) pressing 'anti-stress ball' (inset showing spherical TENG), e) tapping the 'wrist-band' TENG, and f) charging capacitors, g) powering digital calculator and h) thermometer by finger tapping.

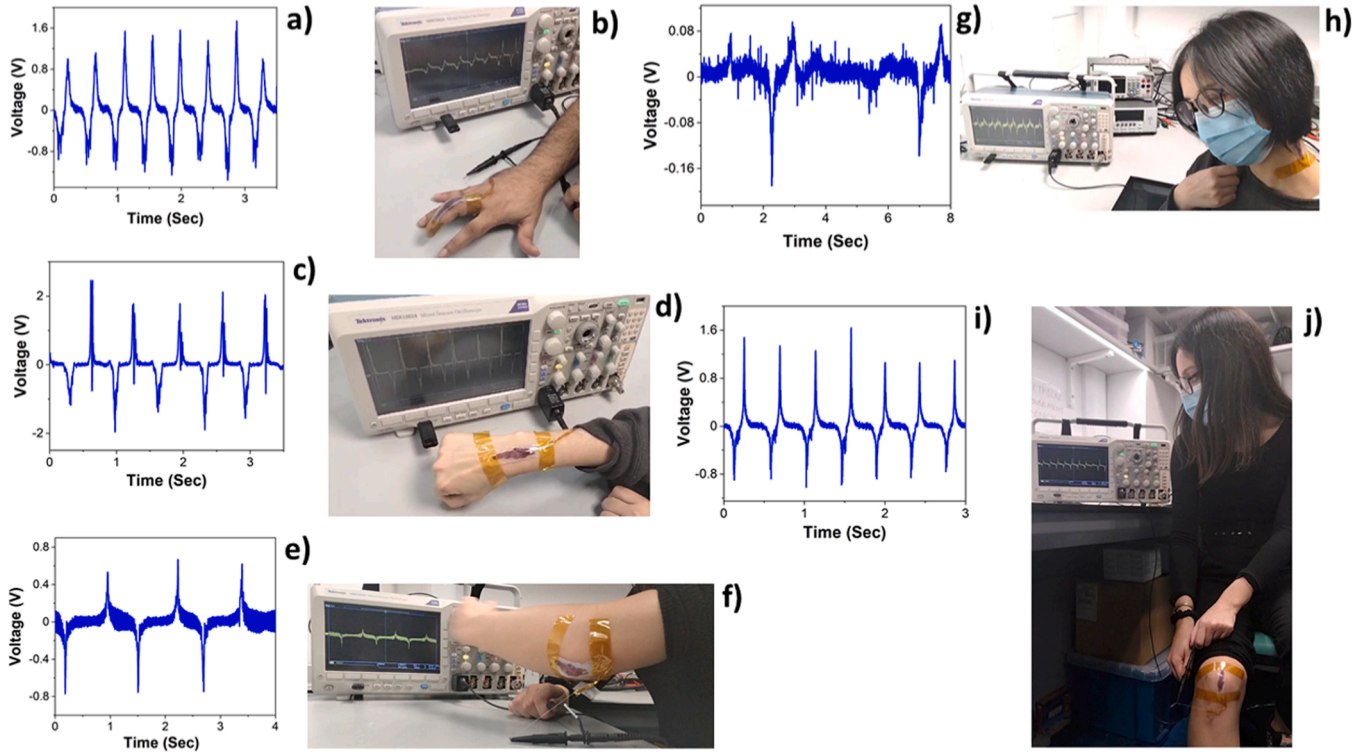

Fig. 7. Demonstration of body movement detection capability of G3 TENG. The graph and the image represent V_{oc} obtained and the corresponding location of TENG on body; a) and b) from finger joint movement, c) and d) wrist bending, e) and f) elbow joint movement, g) and h) neck movement (sideways) and i) and j) knee bending movement.

However, there was no leakage or rupture of the device even at high forces and this is due to the robust yet elastic nature of the TENG. Although, more detailed studies are needed, the TENG shows promise as a soft device for sensing haptic and tactile feedbacks during activities such as surgical procedures and patient (with neuromuscular diseases)-device interactions.

Apart from the energy harvesting capability, we also exploited the TENG as a self-powered door movement sensor based on the human touch or any surface. A TENG strip (size: 10 cm × 1 cm) was attached on the inner side of a door handle (Fig. 8a). As can be seen from the movie (video S13, ESI†), a signal is generated in the whenever the door is opened by touching the handle and this works even with a gloved hand. Thus, the flexible device can be used as self-powered tactile sensor patch on movable objects for surveillance and potential object recognition.

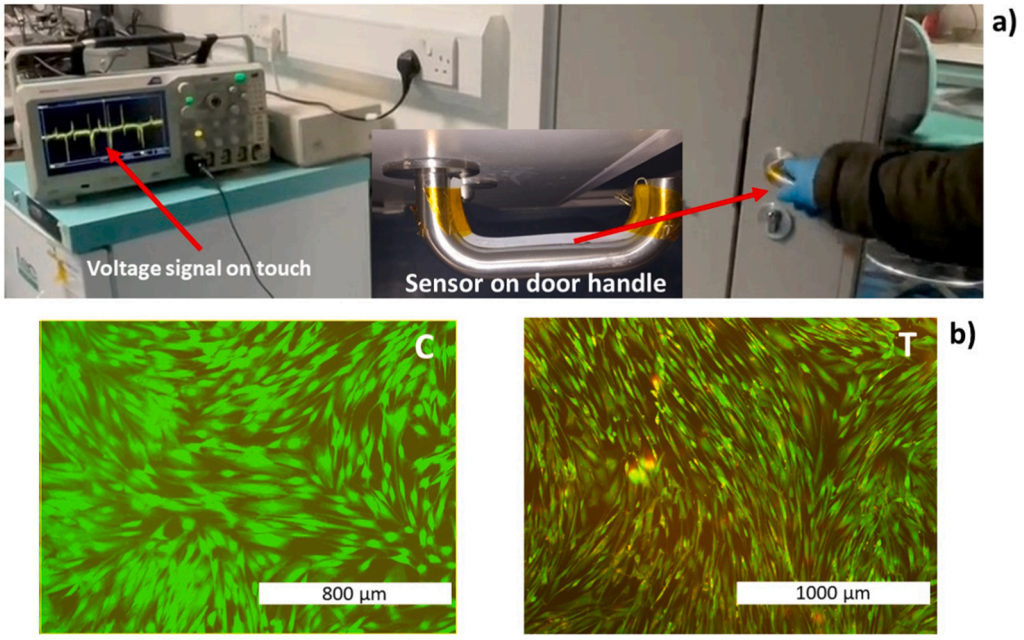

Fig. 8. a) Self-powered door sensor using G3 TENG applied on the door handle (inset showing the flexible TENG strip attached to the inner side of the handle and b) fluorescence microscope image showing biocompatibility of the TENG tested on human dermal fibroblast.

Supplementary material related to this article can be found online at doi:10.1016/j.nanoen.2022.108127.

It is well known that commercial elastomers and hydrogels are routinely used as tissue regeneration scaffolds [30,34,55]. In addition, AuNps are common in various biomedical and drug delivery research owing to their excellent bioactive and antimicrobial properties. Based on the composition of our TENG and future application prospects, it is essential to evaluate biocompatibility. Therefore, we investigated cytotoxicity of the G3 hydrogel on human cell line. To demonstrate biocompatibility, human dermal fibroblasts (HDF) was incubated with a small piece of the gel for 72 h. The concentration of AuNp was 150 μg/mL in a total volume of 3 mL. The cell viability is determined from the proportion of green (live cells) and red (dead cells) which has been dual stained with calcein AM and ethidium homodimer respectively [56]. Fig. 8b shows the fluorescence microscopic images of control (left image-without gel) and treated (right image) HDFs after 72 h incubation. As evident from the right image), predominantly green cells with elongated morphology, characteristic of healthy growing fibroblasts are observed in the treated cells indicating that the hydrogel is not cytotoxic in nature. Although the concentration is AuNp is quite high, the observed non-cytotoxicity is probably due to the entrapment and slow release of nanoparticles in the gel matrix which significantly limits its exposure to the cells. Thus, through these practical demonstrations, the TENG shows a strong potential to be implemented as a self-powered energy source for smart devices related to renewable energy, wearable electronics and implantable sensors.

4. Conclusion

We have designed a soft TENG using a biocompatible triboelectric elastomer and gold nanoparticle doped conducting hydrogel serving as the electrode. The hydrogel electrode is formed by following a green synthetic route which involve in situ synthesis and inclusion of gold nanoparticles inside borate cross-linked PVA hydrogel matrix. This one pot synthesis is scalable and due to the multiple crosslinking interactions between PVA, borate, tannic acid and AuNps, the hydrogel and the resultant TENG offers multifaceted features such as high stretchability (≈ 233%), rapid-self healing, semi-transparency, durability, robustness, and design flexibility. Incorporation of highly conducting AuNps in the hydrogel electrode enables outstanding performance (power density of 1.68 Wm^{-2} and energy conversion efficiency of 26%) by forming conducting pathways in the PVA matrix, which has not been achieved in contemporary hydrogel based TENGs. We demonstrated highly efficient biomechanical energy harvesting from various human body movements, exercises and self-powered sensing capability using the TENG, indicating its potential for use in emerging self-powered electronic skins (E-skins), wearable electronics, soft robotics, and implantable sensors and health monitoring devices.

CRediT authorship contribution statement

Biswajoy Bagchi: Conceptualization, Methodology, Validation, Investigation, Visualization, Writing – original draft. **Priyankan Datta:** Methodology, Investigation, Writing – review & editing. **Carmen Salvadores Fernandez:** Methodology, Writing - review & editing. **Lulu Xu:** Methodology. **Priya Gupta:** Writing – review & editing. **Wei Huang:** Methodology. **Anna L. David:** Writing – review & editing. **Dimitrios Siassakos:** Writing – review & editing. **Shervanthi Homer-Vanniasinkam:** Writing – review & editing. **Manish K. Tiwari:** Supervision, Conceptualization, Investigation, Writing – review & editing, Resources, Funding acquisition.

Declaration of Competing Interest

The authors declare that they have no known competing financial interests or personal relationships that could have appeared to influence the work reported in this paper.

Data Availability

Data will be made available on request.

Acknowledgement

This work is partially supported by the Wellcome/EPSRC Centre for Interventional and Surgical Sciences (WEISS) (203145Z/16/Z), NICE-DROPS project supported by the European Research Council (ERC) under the European Union's Horizon 2020 research and innovation programme under grant agreement no. 714712. MKT also acknowledges Royal Society Wolfson Fellowship.

Appendix A. Supporting information

Supplementary data associated with this article can be found in the online version at doi:10.1016/j.nanoen.2022.108127.

References

[1] S. Wang, X. Mu, Y. Yang, C. Sun, A.Y. Gu, Z.L. Wang, Adv. Mater. 27 (2015) 240.
[2] Z. Zhao, X. Pu, C. Du, L. Li, C. Jiang, W. Hu, Z.L. Wang, ACS Nano 10 (2016) 1780.
[3] Z.L. Wang, J. Chen, L. Lin, Energy Environ. Sci. 8 (2015) 2250.
[4] H.L. Zhang, Y. Yang, Y.J. Su, J. Chen, K. Adams, S. Lee, C.G. Hu, Z.L. Wang, Adv. Funct. Mater. 24 (2014) 1401.
[5] X. He, Y. Zi, H. Guo, H. Zheng, Yi Xi, C. Wu, J. Wang, W. Zhang, C. Lu, Z.L. Wang, Adv. Funct. Mater. 27 (2017) 1604378.
[6] Z.M. Su, M.D. Han, X.L. Cheng, H.T. Chen, X.X. Chen, H.X. Zhang, Adv. Funct. Mater. 26 (2016) 5524.
[7] J. Wang, Y. Li, Z. Xie, Y. Xu, J. Zhou, T. Cheng, H. Zhao, Z.L. Wang, Adv. Energy Mater. 10 (2020) 1904227.
[8] J. Yang, J. Chen, Y. Yang, H.L. Zhang, W.Q. Yang, P. Bai, Y.J. Su, Z.L. Wang, Adv. Energy Mater. 4 (2014) 1301322.
[9] Y. Jie, X. Jia, J. Zou, Y. Chen, N. Wang, Z.L. Wang, X. Cao, Adv. Energy Mater. 8 (2018) 1703133.
[10] Z.C. Quan, C.B. Han, T. Jiang, Z.L. Wang, Adv. Energy Mater. 6 (2016) 1501799.
[11] T. Jiang, H. Pang, J. An, P. Lu, Y. Feng, X. Liang, W. Zhong, Z.L. Wang, Adv. Energy Mater. 10 (2020) 2000064.
[12] J. Zou, M. Zhang, J. Huang, J. Bian, Y. Jie, M. Willander, X. Cao, N. Wang, Z. L. Wang, Adv. Energy Mater. 8 (2018) 1702671.
[13] S.S.K. Mallineni, Y. Dong, H. Behlow, A.M. Rao, R. Podila, Adv. Energy Mater. 8 (2018) 1702736.
[14] C. Wu, A.C. Wang, W. Ding, H. Guo, Z.L. Wang, Adv. Energy Mater. 9 (2019) 1802906.
[15] T. Jing, B. Xu, Y. Yang, M. Li, Y. Gao, Nano Energy 78 (2020), 105373.
[16] X. Han, D. Jiang, X. Qu, Y. Bai, Y. Cao, R. Luo, Z. Li, Materials 14 (2021) 1689.
[17] W. Liao, X. Liu, Y. Li, X. Xu, J. Jiang, S. Lu, D. Bao, Z. Wen, X. Sun, Nano Res. 15 (2021) 2060.
[18] L. Sun, S. Chen, Y. Guo, J. Song, L. Zhang, L. Xiao, Q. Guan, Z. You, Nano Energy 63 (2019), 103847.
[19] Z. Wen, IntechOpen (2020).
[20] W. Paosangthong, R. Torah, S. Beeby, Nano Energy 55 (2019) 401.
[21] D. Bao, Z. Wen, J. Shi, L. Xie, H. Jiang, J. Jiang, Y. Yang, W. Liao, Xuhui Sun, J. Mater. Chem. A 8 (2020) 13787.
[22] X. Jing, H. Li, H.Y. Mi, P.Y. Feng, X. Tao, Y. Liu, C. Liu, C. Shen, J. Mater. Chem. C. 8 (2020) 5752.
[23] F. He, X. You, H. Gong, Y. Yang, T. Bai, W. Wang, W. Guo, X. Liu, M. Ye, ACS Appl. Mater. Interfaces 12 (2020) 6442.
[24] G. Li, L. Li, P. Zhang, C. Chang, F. Xubc, X. Pu, RSC Adv. 11 (2021) 17437.
[25] X. Luo, L. Zhu, Y.C. Wang, J. Li, J. Nie, Z.L. Wang, Adv. Funct. Mater. (2021) 2104928.
[26] X. Pu, M. Liu, X. Chen, J. Sun, C. Du, Y. Zhang, J. Zhai, W. Hu, Z.L. Wang, Sci. Adv. 3 (2017) 1700015.
[27] L. Sun, S. Chen, Y. Guo, J. Song, L. Zhang, L. Xiao, Q. Guan, Z. You, Nano Energy 63 (2019), 103847.
[28] J. Song, S. Chen, L. Sun, Y. Guo, L. Zhang, S. Wang, H. Xuan, Q. Guan, Z. you, Adv. Mater. 32 (2020) 1906994.
[29] S. Jiang, J. Deng, Y. Jin, B. Qian, W. Lv, Q. Zhou, E. Mei, R.E. Neisiany, Y. Liu, Z. you, J. Pan Bioact. Mater. 21 (2022) 313–323.
[30] E.A. Kamoun, E.S. Kenawy, X. Chen, J. Adv. Res 8 (2017) 217.
[31] B. Lu, F. Lin, X. Jiang, J. Cheng, Q. Lu, J. Song, C. Chen, B. Huang, ACS Sustain. Chem. Eng. 5 (1) (2017) 948.
[32] X. Sun, F. Yao, J. Li, J. Mater, Chem. A 8 (2020) 18605.
[33] Y. Yeh, B. Creran, V.M. Rotello, Nanoscale 4 (2012) 1871.
[34] L.A. Dykman, N.G. Khlebtsov, Acta Nat. 3 (2) (2011) 34.
[35] G. Lim, S.S. Kwak, N. Kwon, T. Kim, H. Kim, S.M. Kim, S. Kim, B. Lim, Nano Energy 42 (2017) 300.

[36] S. Park, M. Seol, S. Jeon, D. Kim, D. Lee, Y.K. Choi, Sci. Rep. 5 (2015) 13866.
[37] S. Chen, Z. Wu, C. Chu, Y. Ni, R.E. Neisiany, Z. You, Adv. Sci. 9 (2022) 2105146.
[38] Y. Guo, S. Chen, L. Sun, L. Yang, L. Zhang, J. Lou, Z. You, Adv. Func. Mater. 31 (2021) 2009799.
[39] Y. Jia, Q. Guan, L. Zhang, R.E. Neisiany, N. Yan, Y. Li, Z. You, Sci. China Mater. 65 (9) (2022) 2553.
[40] L. Sun, H. Huang, Q. Ding, Y. Guo, W. Sun, Z. Wu, M. Qin, Q. Guan, Z. You, Adv. Fiber Mater. 4 (2022) 98.
[41] Z. Xu, Y. Gao, J. Li, S. Zhu, K. Meng, W. Yin, H. Zhao, Smart Mater. Med 2 (2021) 134.
[42] Q. Guan, G. Lin, Y. Gong, J. Wang, W. Tan, D. Bao, Y. Liu, Z. You, X. Sun, Z. Wen, Y. Pan, J. Mater. Chem. A 7 (2019) 13948.
[43] S.A. Aromal, D. Philip, Phys. E 44 (2012) 1692.
[44] G. Rezvan, G. Pircheraghi, R. Bagher, J. Appl, Polym. Sci. 135 (45) (2018) 46734.
[45] A. Dixit, D.S. Bag, S.J.S. Kalra, Polymer 119 (2017) 263.
[46] T. Ahmad J. Nanotechnol. 2014, DOI: ⟨https://doi.org/10.1155/2014/954206⟩.
[47] J. Han, T. Lei, Q. Wu, Carbohydr. Polym. 102 (2014) 306.
[48] W. Haiss, N.T.K. Thanh, J. Aveyard, D.G. Fernig, Anal. Chem. 79 (2007) 4215.
[49] J. Liu, Y. Lu, J. Am. Chem. Soc. 126 (39) (2004) 12298.
[50] K.H. Hong, Polym. Bull. 74 (2017) 2861.
[51] Y. Chen, L. Peng, T. Liu, Y. Wang, S. Shi, H. Wang, ACS Appl. Mater. Interfaces 8 (2016) 27199.
[52] Y. Chen, C. Jiao, Y. Zhao, J. Zhang, H. Wang, ACS Omega 3 (9) (2018) 11788.
[53] N. Yang, P. Qi, J. Ren, H. Yu, S. Liu, J. Li, W. Chen, D.L. Kaplan, S. Ling, ACS Appl. Mater. Interfaces 11 (26) (2019) 23632.
[54] K. Chan, D. Yang, B. Demir, A.P. Mouritz, H. Lin, B. Jia, K. Lau, Compos. Part B 178 (2019), 107480.
[55] R. Herbert, J. Kim, Y.S. Kim, H.M. Lee, W. Yeo, Materials 11 (2018) 187.
[56] S. Somodi, R. Guthoff, Ophthalmologe 92 (1995) 452.

Biswajoy Bagchi received his BSc. in Chemistry from Calcutta University and MSc. in Biotechnology and PhD in Material Sciences from Jadavpur University. He is a postdoctoral research fellow at Wellcome-EPSRC Centre for Interventional and Surgical Sciences, University College London (UCL) and jointly works with Mechanical Engineering department (UCL). His research focuses on developing therapeutic antimicrobial nanocomposites and scaffold materials and piezoelectric/triboelectric nanocomposites for biomedical sensors and energy harvesting applications.

Priyankan Datta received his B.Tech. in Electrical Engineering from West Bengal University of Technology and Ph.D. in Mechanical Engineering from Jadavpur University. He is a postdoctoral research scholar at the Nanoengineered Systems Laboratory of Mechanical Engineering Department, University College London (UCL) and jointly works at Wellcome-EPSRC Centre for Interventional and Surgical Sciences, UCL. His research focuses on the development of novel nano-composites to develop smart, self-powered miniaturized flexible sensors for applications in diverse fields like energy harvesting, biomedical sensing and wearable electronics.

Carmen Salvadores Fernandez is a PhD student at the Wellcome-EPSRC Centre for Interventional and Surgical Sciences and part of the Nanoengineered Systems Lab at University College London (UCL). She completed her Mechanical Engineering (MEng) degree in UCL in September 2015. In September 2019, she was awarded the "la Caixa" fellowship to pursue her doctoral research. Her research focuses on the design of advanced nanocomposites for flexible electronics, tactile systems and monitoring devices for healthcare applications.

Lulu Xu is a research fellow at Wellcome-EPSRC Centre for Interventional and Surgical Sciences, University College London (UCL). She received her Ph.D. degree in Textile Science & Technology from the Department of Materials, University of Manchester. Her research interests include additive printing, wearable sensors, e-textiles and wireless communication.

Priya Gupta received her M.Tech degree in VLSI design from Banasthali University, India, and Ph.D. degree in low power IC design from the Birla Institute of technology and Science (BITS) Pilani, India. She has received Marie Sklodowska-Curie Individual Fellowship grant by European Commission for her project "Ultra Low Power Digital Circuits for Wireless Medical Implants (UPDWMI)" associated with University of Edinburgh for two years (2018–2020). Currently, she is working as research fellow at Wellcome-EPSRC Centre for Interventional and Surgical Sciences, in the Department of Medical Physics & Biomedical Engineering, University College London (UCL). Her primary research focuses on mixed signal IC designs at deep micron CMOS technologies for biomedical applications, Flexible Electronics and Wireless Sensing.

Wei Huang is a PhD student at Nanoengineered Systems Laboratory in University College London (UCL). He joined UCL in September 2020. Before that, he received his master's degree in Vehicle Engineering of Beihang University (BUAA) in China. His research deals with the structural and functional (performance) characterization of advanced materials and structures across a wide range of areas. He is particularly interested in understanding how multi-functional materials/composites (self-healing materials) and structures (lattices, adhesive joints, etc.) respond to various loadings.

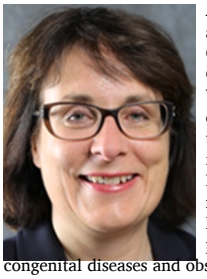

Anna L. David is Professor, Honorary Consultant in Obstetrics and Maternal Fetal Medicine, and Director of the Elizabeth Garrett Anderson Institute for Women's Health, University College London (UCL). She is also a co-investigator for the Wellcome-EPSRC Centre for Interventional and Surgical Sciences at UCL. She is a Fellow of the Royal College of Obstetricians and Gynaecologists (RCOG) and is subspecialty trained in Maternal Fetal Medicine. She was awarded a PhD in Fetal Medicine at UCL in 2015 on fetal gene therapy. Her main research is in translational obstetric and fetal medicine. She leads the Centre for Prenatal Therapy whose aim is to develop prenatal therapies for life threatening disorders such as congenital diseases and obstetric complications such as fetal growth restriction, stillbirth and preterm birth. With UCL engineers at WEISS she is developing novel ways to image the fetus and to improve the safety of birth.

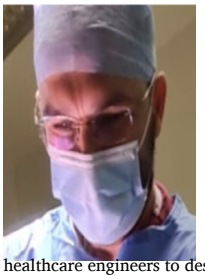

Dimitrios Siassakos is Professor and Honorary Consultant in Obstetrics at University College London and University College Hospital. He was awarded his professorial chair in 2020–2021. His clinical work is devoted to managing labour ward, and to looking after women with previous adverse pregnancy outcome, to optimize their chance of a healthy subsequent pregnancy. He has led the development and dissemination of regional, national, and global training courses to improve management of obstetric emergencies (PROMPT, SMASH), operative birth (ROBUST, ART&CRAFT), As Deputy Medical Director for the Wellcome/EPSRC centre for Intervention and Surgical Sciences (WEISS), Dimitrios is working closely with healthcare engineers to design novel tools that aim to improve the safety of birth.

Shervanthi Homer-Vanniasinkam is Professor of Engineering & Surgery at University College London and Founding Professor of Surgery at the University of Warwick Medical School & University Hospitals Coventry and Warwickshire, and She is a Consultant Vascular Surgeon at Leeds Teaching Hospitals NHS Trust. She is also the Founding Director of EXSEL (a novel medical student scholarship scheme), at the University of Leeds Medical School. She has an outstanding track record of national (Universities of Leeds, London, Warwick) and international (Harvard, Yale, Singapore, India, Sri Lanka) collaborative and translation oriented research. She is a Visiting Scholar at Harvard University, the Yeoh Ghim Seng Visiting Professor of Surgery at the National University of Singapore and the Brahm Prakash Visiting Professor at the Indian Institute of Science.

Manish K Tiwari is a Professor of Nanoengineering and Royal Society Wolfson Fellow in the Mechanical Engineering Department of the University College London. He is also a Supervisor at Wellcome-EPSRC Centre for Interventional and Surgical Sciences at UCL. He received his PhD from the University of Illinois at Chicago (UIC) in 2009. After graduating, he did his postdoctoral research in the Laboratory of Thermodynamics in Emerging Technologies at ETH Zurich. Prof. Tiwari's research focuses on interfaces - encompassing broad areas of small scale manufacturing and transport phenomena with an emphasis on developing new energy and healthcare technologies.